SLGNet: Synergizing Structural Priors and Language-Guided Modulation for Multimodal Object Detection

Xiantai Xiang, Guangyao Zhou, Zixiao Wen, Wenshuai Li, Ben Niu‡, Feng Wang, Lijia Huang, Qiantong Wang, Yuhan Liu, Zongxu Pan, *Senior Member, IEEE* and Yuxin Hu

Abstract—Multimodal object detection leveraging RGB and Infrared (IR) images is pivotal for robust perception in all-weather scenarios. While recent adapter-based approaches efficiently transfer RGB-pretrained foundation models to this task, they often prioritize model efficiency at the expense of cross-modal structural consistency. Consequently, critical structural cues are frequently lost when significant domain gaps arise, such as in high-contrast or nighttime environments. Moreover, conventional static multimodal fusion mechanisms typically lack environmental awareness, resulting in suboptimal adaptation and constrained detection performance under complex, dynamic scene variations. To address these limitations, we propose SLGNet, a parameter-efficient framework that synergizes hierarchical structural priors and language-guided modulation within a frozen Vision Transformer (ViT)-based foundation model. Specifically, we design a Structure-Aware Adapter to extract hierarchical structural representations from both modalities and dynamically inject them into the ViT to compensate for structural degradation inherent in ViT-based backbones. Furthermore, we propose a Language-Guided Modulation module that exploits VLM-driven structured captions to dynamically recalibrate visual features, thereby endowing the model with robust environmental awareness. Extensive experiments on the LLVIP, FLIR, KAIST, and DroneVehicle datasets demonstrate that SLGNet establishes new state-of-the-art performance. Notably, on the LLVIP benchmark, our method achieves an mAP of 66.1, while reducing trainable parameters by approximately 87% compared to traditional full fine-tuning. This confirms SLGNet as a robust and efficient solution for multimodal perception.

Index Terms—Multimodal Object Detection, Adapter Tuning, Vision-Language Models

I. INTRODUCTION

Robust object detection in dynamic, open-world environments is a cornerstone of intelligent autonomous systems, particularly in autonomous driving and unmanned aerial vehicle (UAV)-based remote sensing [1]–[3]. While visible (RGB) sensors provide rich texture and color information under favorable lighting, their performance degrades significantly in low-light, foggy, or cluttered scenarios [4]–[6]. Conversely, thermal infrared (IR) sensors capture object emissivity and are immune to illumination variations, yet they lack textural detail and are susceptible to thermal crossover [7]. Consequently, integrating

‡ indicates the corresponding author.

The authors are with the Aerospace Information Research Institute, Chinese Academy of Sciences, Beijing 100190, China, also with the Key Laboratory of Target Cognition and Application Technology, Chinese Academy of Sciences, Beijing 100190, China, and also with the School of Electronic, Electrical and Communication Engineering, University of Chinese Academy of Sciences, Beijing 101408, China (email: xiangxiantai23@mails.ucas.ac.cn).

Zongxu Pan is with the School of Software Engineering, Xi'an Jiaotong University, Xi'an 710049, China (email:panzx@xjtu.edu.cn).
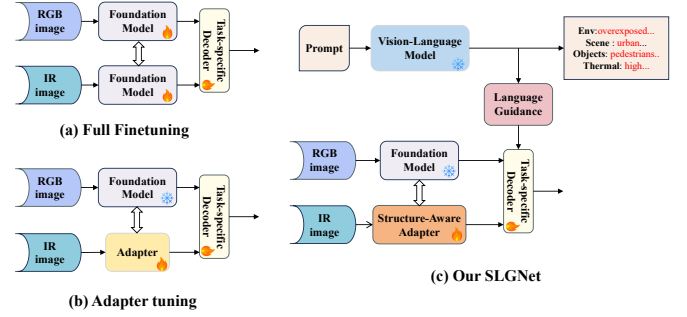
Fig. 1. Comparison of multimodal adaptation paradigms: Existing strategies vs. our SLGNet. (a) Full Fine-tuning: Updates all parameters of the foundation model, leading to high computational costs and potential catastrophic forgetting. (b) Standard Adapter Tuning: Freezes the backbone and trains lightweight adapters. However, these methods often lack explicit structural constraints, leading to spatial detail loss. (c) SLGNet (Ours): We propose a synergistic framework that incorporates a Structure-Aware Adapter to preserve geometric details (bottom) and Language-Guided Modulation (top) to enhance semantic adaptability. The ❄ and 🔥 icons indicate frozen and trainable parameters, respectively.

the complementary strengths of RGB and IR modalities has emerged as a pivotal research direction, with the primary goal of achieving reliable all-weather perception [8], [9].

Recent advancements in computer vision have been dominated by Vision Transformers (ViTs), particularly large-scale foundation models pre-trained on massive RGB datasets (e.g., DINO Series, SAM) [10]–[14]. Transferring these powerful representations to the RGB-IR domain offers a promising path to surpass traditional detectors [3], [15], [16]. However, due to the scarcity of large-scale infrared foundation models, current research focuses on adapting RGB baselines to multimodal data. As illustrated in Fig. 1(a), a straightforward approach is **Full Fine-tuning (FFT)** or designing heavy fusion architectures. For instance, M2FP [17] addresses domain bias by pretraining modality-specific backbones via masked reconstruction, yet it fundamentally relies on the Full Fine-tuning (FFT) paradigm to adapt these pre-trained weights to downstream drone-based RGB-T tasks. Similarly, other conventional methods directly fine-tune RGB-pretrained models on RGB-IR datasets to establish semantic relevance [4]. Despite their effectiveness, these paradigms are computationally prohibitive and prone to catastrophic forgetting, where the model loses its robust general-purpose features [18]. To mitigate this, **Adapter Tuning** (Fig. 1(b)) has emerged as a parameter-efficient alternative [19], [20]. UniRGB-IR [16], for example, proposes a scalable framework that introduces a novel adapter

mechanism to incorporate multimodal features into frozen backbones effectively. While efficient, conventional adapters typically prioritize semantic feature alignment and often neglect the structural degradation resulting from the inherent spatial resolution reduction in ViTs. This loss of fine-grained geometric details is particularly critical in remote sensing tasks, where distinguishing small, densely packed objects (e.g., vehicles in aerial views) relies heavily on precise spatial cues. As the domain gap widens, these methods struggle to preserve critical high-frequency cues (e.g., edges and contours). To bridge this gap, as depicted in the bottom branch of Fig. 1(c), we propose a **Structure-Aware Adapter**. This component is explicitly designed to capture hierarchical structural priors from both modalities, ensuring that geometric integrity is maintained alongside semantic adaptation.

Beyond structural degradation, a critical bottleneck lies in the fusion mechanism itself. Most existing multimodal approaches predominantly utilize static fusion strategies, including element-wise addition, concatenation, or visual-attention mechanisms [21]–[23]. These methods apply a uniform policy across all input pairs, essentially ignoring varying modality contributions under changing environmental conditions. As implicitly depicted in Fig. 1(a) and (b), such networks lack explicit mechanisms to perceive scene dynamics, instead relying on fixed weights to fuse features even when one modality is severely degraded. Consequently, this environment-agnostic paradigm often allows noise from a degraded sensor (e.g., an overexposed background) to contaminate the final representation. Although some methods attempt to weight modalities via attention modules [8], [24], they effectively lack the high-level semantic reasoning capabilities required to explicitly interpret scene attributes. To address this, as shown in the top branch of Fig. 1(c), we introduce a **Language-Guided Modulation (LGM)** module. Unlike static approaches, LGM exploits semantic reasoning to explicitly interpret scene dynamics, empowering the model to "read" the environment and adapt its fusion strategy accordingly.

Conjoining these structural and semantic insights, we present **SLGNet**, a parameter-efficient framework that synergizes structural priors and language-guided modulation within a frozen ViT-based foundation model. Our approach is built upon the premise that robust multimodal detection demands both hierarchical geometric guidance and high-level environmental awareness. Rather than disrupting the pre-trained feature space via full fine-tuning, SLGNet decouples the adaptation process into two complementary streams. Specifically, the Structure-Aware Adapter remedies structural degradation by injecting hierarchical structural priors into the transformer layers, ensuring precise localization. Simultaneously, the Language-Guided Modulation (LGM) module interprets scene dynamics via VLM reasoning to dynamically recalibrate feature channels, enabling the adaptive prioritization of informative modalities across diverse environments. This dual-stream design allows SLGNet to retain the generalization power of the foundation model while efficiently adapting to the nuances of RGB-IR perception.

The main contributions of this work are summarized as follows:

- We propose SLGNet, a novel adapter-tuning framework that effectively transfers the capability of frozen RGB foundation models to multimodal object detection. It achieves a superior balance between detection accuracy and training efficiency, significantly outperforming full fine-tuning paradigms.
- We design a Structure-Aware Adapter that explicitly remedies the structural degradation inherent in ViTs by extracting and injecting hierarchical structural priors. This mechanism preserves geometric integrity and enhances localization precision, particularly for structure-sensitive targets in aerial remote sensing.
- We introduce a Language-Guided Modulation (LGM) module that exploits VLM-driven structured captions to dynamically recalibrate visual features. This mechanism endows the model with high-level environmental awareness, enabling robust adaptation to dynamic illumination and thermal variations.
- Extensive experiments on four benchmark datasets (LLVIP, FLIR, KAIST, and DroneVehicle) demonstrate that SLGNet achieves state-of-the-art performance. Notably, on the LLVIP benchmark, our method achieves an mAP of 66.1, while reducing trainable parameters by approximately 87% compared to full fine-tuning counterparts.

II. RELATED WORK

A. Multimodal Object Detection

Multimodal object detection, specifically the synergistic fusion of RGB and Thermal Infrared (IR) data, is critical for all-weather remote sensing perception [8], [25], [26]. Early research predominantly relied on CNN-based architectures, where pioneering works explored distinct fusion stages [5], [7] or introduced specific mechanisms such as illumination-aware weighting [27], [28] and spatial alignment modules [29], [30] to mitigate sensor parallax. While these methods often struggle with long-range dependencies, the field has recently shifted towards Vision Transformers (ViTs) and State Space Models (SSMs) for global context modeling [31], [32]. Representative frameworks, such as C2Former [33] and CrossModalNet [22], utilize inter-modality cross-attention to achieve fine-grained semantic alignment. In contrast, Mamba-based approaches, including WaveMamba [9] and DMM [34], leverage advanced wavelet transforms or disparity guidance to address frequency and spatial discrepancies in complex aerial imagery.

Despite these architectural evolutions, current paradigms face two critical limitations. First, the reliance on Full Fine-Tuning (FFT) for heavy backbones incurs high computational and storage costs, which hinders deployment on resource-constrained edge devices like UAVs. Second, existing fusion strategies remain largely static and lack the high-level semantic reasoning required to interpret complex environmental dynamics, such as distinguishing sensor overexposure from nighttime. To overcome these challenges, our SLGNet introduces a parameter-efficient, language-driven modulation paradigm that synergizes structural recovery with semantic awareness.

B. Parameter-Efficient Transfer Learning

Parameter-Efficient Transfer Learning (PETL) aims to adapt frozen foundation models to downstream tasks via lightweight modules, drastically reducing storage and computational costs. Initially popularized in NLP through architectures like Adapters [35] and LoRA [36], this paradigm has been extensively explored in computer vision through diverse mechanisms. For instance, Visual Prompt Tuning (VPT) [37] prepends learnable tokens to the input sequence to modulate attention, while LoRA-based methods [38] optimize low-rank decomposition matrices to approximate weight updates. Among these, Adapter-based approaches [19], [20], [39] inject lightweight bottleneck modules within transformer layers, proving particularly effective for dense prediction tasks by preserving feature map integrity. Recent studies have further extended this to multimodal domains, such as UniRGB-IR [16], to bridge modality gaps without updating the heavy backbone. However, despite their efficiency, most existing approaches prioritize semantic alignment while neglecting the spatial information loss inherent in frozen ViT backbones (typically downsampled to $1/16$). Unlike full fine-tuning, standard adapters struggle to recover high-frequency cues (e.g., edges) lost during patch embedding, leading to suboptimal localization. To bridge this gap, our Structure-Aware Adapter is explicitly designed to inject multi-scale structural priors into the frozen feature space.

C. Vision-Language Models for Scene Understanding

Large-scale Vision-Language Models (VLMs) have revolutionized representation learning, where foundation models such as CLIP [40], ALIGN [41], and BLIP [42] establish robust cross-modal alignment, further advanced by Large Multimodal Models (LMMs) like LLaVA [43], MiniGPT-4 [44], and Qwen-VL [45] for complex reasoning. In object detection, this paradigm facilitates Open-Vocabulary Detection (OVD), utilizing text embeddings as dynamic classifiers in approaches like GLIP [46], GroundingDINO [47], and RegionCLIP [48]. Crucially, this trend has extended to the remote sensing domain, yielding specialized foundation models such as RemoteCLIP [49], GeoChat [50], SkySense [51], and RSGPT [52] for aerial image captioning and retrieval.

However, despite this proliferation, the potential of VLMs to act as high-level "scene interpreters" for optimizing low-level feature fusion remains largely unexplored. Existing multimodal detectors [3], [24] typically treat fusion as a static signal processing problem. Existing methods often neglect semantic environmental contexts such as severe overexposure or thermal crossover. While VLMs easily identify these attributes, traditional CNN and ViT encoders struggle to formulate such complex dynamics explicitly. To address this, our Language-Guided Modulation (LGM) module leverages the reasoning power of frozen VLMs to explicitly infer these scene attributes, using linguistic priors to globally recalibrate visual features for robust environmental adaptation.

III. THE PROPOSED METHOD

As illustrated in Fig. 2, we propose SLGNet, a parameter-efficient multimodal detection framework that synergizes a frozen Vision Transformer (ViT) with structure-aware and language-guided adaptations.

Specifically, the overall pipeline proceeds as follows: Given an input RGB image, the frozen ViT backbone first divides it into non-overlapping patches and projects them into a sequence of visual embeddings. As these tokenized representations propagate through the transformer layers, the network maintains a spatial reduction ratio of $1/16$ relative to the input resolution. To compensate for the potential loss of high-frequency details at this scale, the Structure-Aware Adapter (Sec. III-A) extracts hierarchical structural priors (e.g., edges) from both RGB and IR modalities. These priors are processed via MLPs and dynamically injected into the ViT stages through *Feature Fusion Adapter (FF-Adapter)*.

Subsequently, the Language-Guided Modulation (LGM) (Sec. III-B) recalibrates the output of the ViT backbone by leveraging semantic insights from a Vision-Language Model (VLM). As illustrated in the top branch of Fig. 2, the VLM generates structured captions encompassing four distinct dimensions: Environment, Scene, Objects, and Thermal. These linguistic priors are then utilized to globally recalibrate the visual representations via affine transformations (γ, β). Finally, the resulting feature maps, now enriched with both structural integrity and semantic context, are forwarded to the task-specific decoder for robust object detection.

To leverage the robust visual representations of the ViT backbone pre-trained on large-scale RGB datasets while mitigating catastrophic forgetting, we adopt an adapter tuning paradigm. Unlike full fine-tuning which updates all parameters θ, we decouple the model parameters into two disjoint sets: $\theta = \{\theta_{\text{vit}}, \theta_{\text{adapter}}\}$. Here, θ_{vit} denotes the frozen backbone parameters, and $\theta_{\text{adapter}} = \{\theta_{\text{struc}}, \theta_{\text{lang}}\}$ represents the lightweight learnable parameters introduced by our Structure-Aware Adapter and Language-Guided Modulation modules. During training, we optimize only θ_{adapter} by minimizing the task loss:

$$\theta_{\text{adapter}} \leftarrow \arg\min_{\theta_{\text{adapter}}} \sum_{j=1}^{M} \mathcal{L}(F_{\theta_{\text{vit}}, \theta_{\text{adapter}}}(x_j), y_j) \tag{1}$$

where this constrained optimization ensures efficient adaptation to multimodal tasks $(| \theta_{\text{adapter}} | \ll | \theta_{\text{vit}} |)$ without disrupting the foundation model's feature space.

A. Structure-Aware Adapter

In this section, we detail the *Structure-Aware Adapter* (SA-Adapter), a pivotal component of the SLGNet framework designed to enhance cross-modal interaction while preserving hierarchical structural priors, such as edges and object contours. The adapter comprises two integral modules: the *Structure Encoder* (S-Encoder) and the *Feature Fusion Adapter* (FF-Adapter).

The S-Encoder is tasked with extracting hierarchical structural representations from both RGB and IR modalities. Since the frozen ViT backbone operates at a coarse spatial resolution of $1/16$, recovering these essential hierarchical geometric details is crucial for maintaining structural integrity. Subsequently, the FF-Adapter utilizes a hierarchical sparse
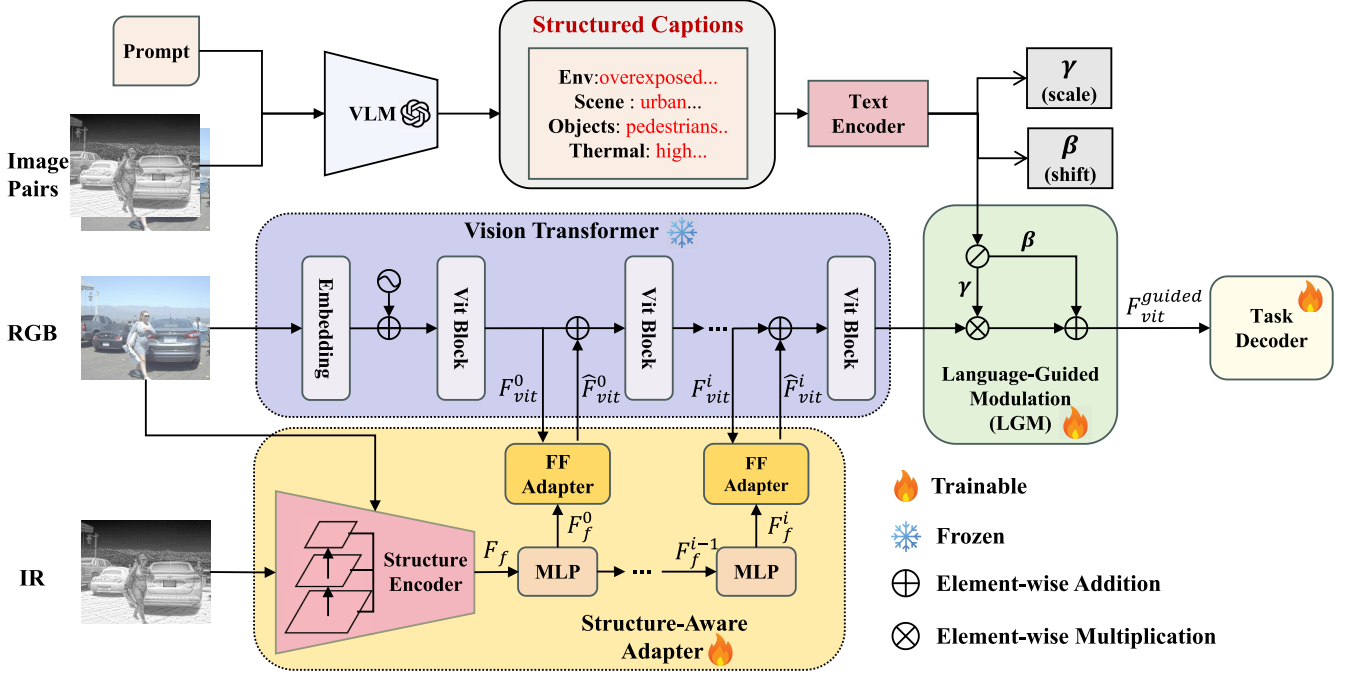
Fig. 2. Overview of the proposed **SLGNet** framework. The architecture synergizes a frozen Vision Transformer (ViT) backbone with two lightweight trainable modules: (1) the **Structure-Aware Adapter** (bottom), which extracts hierarchical structural priors from paired images via a Structure Encoder and injects them into ViT blocks using Feature Fusion Adapter (FF-Adapter); and (2) the **Language-Guided Modulation (LGM)** (right), which utilizes VLM-generated structured captions (Environment, Scene, Objects, Thermal) to recalibrate the final feature map via affine transformations (γ, β). The ❄ and 🔥 icons indicate frozen and trainable parameters, respectively.
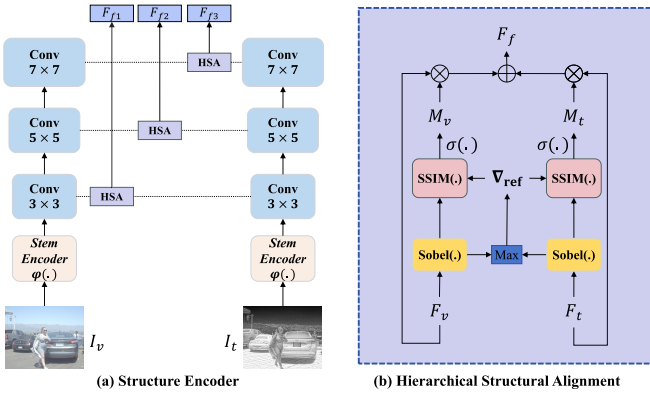

Fig. 3. Detailed architecture of the Structure Encoder. **(a)** The encoder employs progressive convolutional stages to extract hierarchical structural priors across multiple resolutions. **(b)** The Hierarchical Structural Alignment (HSA) module. It establishes a reference structural map ∇_{ref} and utilizes an SSIM-driven mechanism to dynamically weight multimodal features based on their hierarchical structural consistency.

attention mechanism to integrate these priors into the ViT backbone seamlessly. This design ensures effective multimodal alignment without disrupting the pre-trained feature space. Together, these components enable a robust, structure-preserving synergy of complementary modalities, significantly improving object detection performance in complex, dynamic environments.

1) Structure Encoder: The *Structure Encoder* (S-Encoder) is designed to extract hierarchical structural priors from both RGB and IR inputs by leveraging progressive convolutional

stages and a hierarchical structural alignment mechanism. As illustrated in Fig. 3(a), given an RGB image I_v and an IR image I_t, we first extract initial feature representations F_v and F_t using a shared stem encoder $\varphi(\cdot)$. These features are subsequently processed through three sequential convolutional layers with varying kernel sizes of 3×3, 5×5, and 7×7. This hierarchical design yields feature maps F_{vl} and F_{tl} $(l = 1, 2, 3)$ at progressively coarser resolutions $(1/8, 1/16,$ and $1/32$ of the input size), ensuring the capture of both local textures and global geometric cues.

To effectively fuse these multimodal features while preserving object integrity, we introduce a Hierarchical Structural Alignment (HSA) module (see Fig. 3(b)). For each scale l, we first employ the Sobel operator to compute the gradient magnitude, extracting edge responses from both modalities:

$$\nabla F_{vl} = \text{Sobel}(F_{vl}), \quad \nabla F_{tl} = \text{Sobel}(F_{tl}). \quad (2)$$

These edge maps are then aggregated via an element-wise maximum operation to establish a robust reference structural map:

$$\nabla_{\text{ref}} = \max(\nabla F_{vl}, \nabla F_{tl}). \quad (3)$$

Subsequently, we quantify the structural alignment between each modality and this reference utilizing a modified SSIM formulation. As shown in the detailed module diagram, this process incorporates both first-order (mean) and second-order

(variance/covariance) statistics:

$$M'_v = \frac{(2\mu_v\mu_{\text{ref}} + \xi_1)(2\sigma(v, \text{ref}) + \xi_2)}{(\mu_v^2 + \mu_{\text{ref}}^2 + \xi_1)(\sigma_v^2 + \sigma_{\text{ref}}^2 + \xi_2)} \tag{4}$$

$$M'_t = \frac{(2\mu_t\mu_{\text{ref}} + \xi_1)(2\sigma(t, \text{ref}) + \xi_2)}{(\mu_t^2 + \mu_{\text{ref}}^2 + \xi_1)(\sigma_t^2 + \sigma_{\text{ref}}^2 + \xi_2)}, \tag{5}$$

where μ, σ, and $\sigma(\cdot, \cdot)$ denote the mean, variance, and co-variance of the feature maps and the reference, respectively. $\xi_1 = (k_1 L)^2$ and $\xi_2 = (k_2 L)^2$ are stability constants.

The derived similarity scores are then normalized via a Sigmoid function ($\sigma(\cdot)$) to serve as adaptive alignment weights M_v and M_t. The final fused feature at each scale is computed as:

$$F_{f_l} = \sigma(M'_v) \cdot F_{vl} + \sigma(M'_t) \cdot F_{tl}, \quad l \in \{1, 2, 3\}. \tag{6}$$

This mechanism ensures that the encoder dynamically prioritizes the modality with superior structural definition (i.e., higher correlation with ∇_{ref}), maintaining consistency across diverse lighting conditions.

Finally, to align the fused features with the latent space of the frozen ViT, each output F_{f_l} undergoes a 1×1 convolution, projecting its channel dimension to match the ViT token dimension D. These projected structural priors are subsequently injected into the backbone via the FF-Adapters to enrich the visual representation.

2) Feature Fusion Adapter: The *Feature Fusion Adapter* (FF-Adapter) facilitates the seamless injection of hierarchical structural priors into the frozen ViT backbone while addressing the spatial misalignment and resolution discrepancies between 1D tokens and 2D hierarchical features. Drawing inspiration from the deformable attention paradigm [53], we employ a Hierarchical Sparse Attention mechanism to enable each ViT stage to sparsely attend to the most informative spatial locations across levels. Specifically, for the i-th ViT stage, the refined tokens $\hat{F}_{\text{vit}}^{(i)}$ are obtained by:

$$\hat{F}_{\text{vit}}^{(i)} = F_{\text{vit}}^{(i)} + \text{Attn}_{\text{sparse}}\left(F_{\text{vit}}^{(i)}, \left\{F_{f_l}^{(i)} \mid l = 1, 2, 3\right\}\right) \tag{7}$$

where $\{F_{f_l}^{(i)}\}$ represents the structural priors at $1/8$, $1/16$, and $1/32$ resolutions. The sparse attention operation is formulated as:

$$\text{Attn}_{\text{sparse}}(f_q, \{F_{f_l}\}) = \sum_{l=1}^{3} \sum_{k=1}^{K} A_{lqk} W_v F_{f_l}(\phi_l(p_q) + \Delta p_{lk}) \tag{8}$$

Here, for each query token f_q at a reference coordinate p_q, the function $\phi_l(p_q)$ maps the normalized coordinate to the specific resolution of the l-th feature map. Crucially, Δp_{lk} and A_{lqk} denote the learnable sampling offsets and normalized attention weights for the k-th sampling point at the l-th hierarchical level, respectively. By focusing on a small set of K key sampling points rather than the entire feature map, the mechanism achieves efficient cross-level interaction while adaptively capturing critical structural details, such as object boundaries, even if they are spatially distant from the query token.

Furthermore, to ensure alignment with the progressively deepening semantics of the ViT, these hierarchical features are dynamically evolved across stages via a Multi-Layer Perceptron (MLP):

$$\{F_{f_l}^{(i)}\} = \text{MLP}(\{F_{f_l}^{(i-1)}\}) \tag{9}$$

This stage-wise evolution ensures an optimal synergy between the hierarchical visual structure and the changing abstraction levels of the backbone.

B. Language-Guided Modulation

To empower the detection framework with high-level scene understanding and adaptability, we introduce the Language-Guided Modulation (LGM) mechanism. Unlike traditional methods that rely solely on visual statistics, LGM leverages the reasoning capabilities of a Vision-Language Model (VLM) to explicitly modulate the fusion of RGB and IR features using natural language descriptions.

Given a pair of aligned images $(I_{\text{RGB}}, I_{\text{IR}})$, we first employ the Qwen2.5-VL [45] model to generate a comprehensive, structured caption of the scene. As shown in Fig. 2, this structured caption is organized into four distinct contextual components to provide specific linguistic priors:

- **Environmental Context** (s_{env}): Describes global attributes such as lighting (e.g., "dimly lit", "overexposed") and weather conditions.
- **Scene Type** (s_{type}): Categorizes the spatial structure, distinguishing between indoor/outdoor settings or functional areas.
- **Object Density** (s_{obj}): Identifies the presence and distribution of key objects (e.g., "crowded", "sparse").
- **Thermal Signature** (s_{therm}): Interprets infrared cues to describe thermal contrast and temperature variations.

The resulting structured linguistic representation is denoted as $\{s_i\}_{i \in \mathcal{S}}$, where $\mathcal{S} = \{\text{env}, \text{type}, \text{obj}, \text{therm}\}$.

These textual descriptions are subsequently encoded into the latent feature space using the frozen Text Encoder of the CLIP model [40]. This step leverages CLIP's pre-trained alignment to extract robust semantic embeddings without requiring fine-tuning. The feature extraction is formulated as:

$$F_{t_i} = \mathcal{CLIP}_{\text{text}}(s_i) \in \mathbb{R}^{L \times d} \tag{10}$$

where L denotes the sequence length (typically 77 tokens) and d is the embedding dimension. To synthesize these disparate priors, we concatenate the four feature sets along the channel dimension and employ a lightweight Multi-Layer Perceptron (MLP) to project them back to the original dimension d, fusing the information while maintaining the token sequence structure:

$$F_t^{\text{sem}} = \text{MLP}_{\text{proj}}\left(\text{Concat}(F_{t_{\text{env}}}, F_{t_{\text{type}}}, F_{t_{\text{obj}}}, F_{t_{\text{therm}}})\right) \in \mathbb{R}^{L \times d} \tag{11}$$

The core of the LGM mechanism is to use these fused structured caption priors to recalibrate the visual features via affine modulation dynamically. To bridge the domain gap between the text sequence and the visual channels, we first aggregate the text tokens (e.g., via global average pooling) and then pass them through two parallel projection heads to generate channel-wise modulation parameters:

$$\gamma = \text{MLP}_\gamma(\text{Pool}(F_t^{\text{sem}})), \quad \beta = \text{MLP}_\beta(\text{Pool}(F_t^{\text{sem}})) \tag{12}$$

where $\gamma \in \mathbb{R}^C$ and $\beta \in \mathbb{R}^C$ represent the scaling factors and bias terms, respectively. Let the final output of the ViT backbone be $F_{\text{vit}} \in \mathbb{R}^{C \times H \times W}$. We apply a channel-wise affine transformation to inject the language-guided context into the visual representation:

$$F_{\text{vit}}^{\text{guided}} = (\gamma + 1) \cdot F_{\text{vit}} + \beta \tag{13}$$

Here, "$\cdot$" denotes element-wise multiplication. The term $(\gamma + 1)$ incorporates a residual identity connection, ensuring that the modulation gently refines the pre-trained visual features based on the language-driven priors (e.g., suppressing noise in foggy conditions or enhancing thermal targets) rather than distorting them.

IV. EXPERIMENTS

A. Datasets and Metrics

1) Datasets: To comprehensively evaluate the robustness and generalization capability of SLGNet under diverse real-world conditions, we conduct experiments on four distinct multimodal benchmarks: LLVIP [54], FLIR [55], KAIST [1], and DroneVehicle [2].

LLVIP [54]: Designed specifically for low-light vision, this dataset contains 15,488 strictly aligned RGB-IR image pairs (12,025 for training, 3,463 for testing). Most scenes are captured in very dark environments where pedestrians are barely visible in the RGB modality but prominent in the thermal modality. This serves as a critical benchmark for evaluating the effectiveness of our Language-Guided Modulation in enhancing feature discriminability when visual cues are degraded.

FLIR [55]: This dataset focuses on complex outdoor driving scenarios, comprising 10,228 images (8,862 training, 1,366 testing) with annotations for *Person, Car, Bicycle, and Dog*. It is characterized by crowded streets, significant scale variations, and cluttered backgrounds. These conditions pose a substantial challenge to the model's ability to preserve structural details and distinguish objects in dense environments.

KAIST [1]: Containing 95k color-thermal pairs (7,601 for training, 2,252 for testing) captured across day and night, this dataset is widely used to test robustness. A key challenge of KAIST is the inherent *spatial misalignment* between RGB and IR sensors, along with varying illumination conditions. Evaluating on KAIST verifies our Structure-Aware Adapter's ability to perform robust fusion even when spatial correspondence is not perfectly pixel-aligned.

DroneVehicle [2]: Unlike the ground-view datasets above, DroneVehicle consists of 56,878 image pairs collected by UAVs, featuring an aerial perspective. It covers five vehicle categories (*Car, Truck, Bus, Van, Freight-Car*) and provides oriented bounding box annotations. The dataset introduces unique challenges such as small object scales, high density, and complex background textures, setting a high standard for evaluating the adaptability of multimodal detectors in aerial surveillance scenarios.

2) Metrics: For the LLVIP, FLIR, and DroneVehicle datasets, we adopt the standard mean Average Precision (mAP) as the primary evaluation metric, specifically reporting mAP_{50}. For the DroneVehicle dataset, the mAP is calculated based on the Intersection over Union (IoU) of rotated bounding boxes. For the KAIST dataset, following the standard pedestrian detection protocol, we report the log-average miss rate over the range of $[10^{-2}, 10^0]$ False Positives Per Image, denoted as MR^{-2}. Note that for mAP, higher scores indicate better performance, whereas for MR^{-2}, lower scores are better.

B. Implementation Details

1) Network Architecture and Frameworks: We implement SLGNet using the MMDetection framework for horizontal bounding box detection tasks (LLVIP, FLIR, KAIST) and the MMRotate framework for oriented object detection (DroneVehicle). The backbone is based on the standard ViT-Base architecture, initialized with pre-trained weights from DINOv2 [12]. Utilizing DINOv2 is critical as its self-supervised training on large-scale data provides robust geometric and semantic features that align well with our structure-aware design. The proposed Structure-Aware Adapter is inserted before each of the 12 transformer blocks to ensure continuous structural reinforcement throughout the feature extraction process.

2) Training Settings: All models are trained on NVIDIA H20 GPUs. The training process spans 50 epochs with a batch size of 8. We employ the AdamW optimizer with an initial learning rate of 1×10^{-4} and a weight decay of 0.1. To optimize the frozen-backbone paradigm effectively, we utilize a layer-wise learning rate decay strategy with a decay rate of 0.7. This ensures that the lower layers of the adapter retain more generic features while higher layers adapt more aggressively to the specific task. Furthermore, we employ Automatic Mixed Precision (AMP) training to reduce memory consumption and accelerate computation without compromising performance.

3) Inference Strategy: Considering that environmental contexts (e.g., illumination, weather) remain temporally consistent over short durations, we envision an asynchronous inference architecture for real-world deployment. To simulate this, the VLM-based context generation was performed offline in our experiments. This setup reflects a practical scenario where the heavy VLM runs periodically (e.g., every minute) to update modulation parameters, while the visual detector operates in real-time without latency bottlenecks.

C. Comparisons With State-of-The-Art Methods

1) Comparisons on LLVIP Dataset: Table I presents the quantitative comparison of various object detection methods on the LLVIP dataset. This benchmark is specifically designed for low-light scenarios where RGB inputs are severely degraded, making effective cross-modal fusion essential. We compare SLGNet with a wide range of baselines, including unimodal detectors (FasterRCNN, RetinaNet, YOLOv8, and DDQ-DETR) and state-of-the-art multimodal fusion frameworks (ICAFusion, RSDet, UniRGB-IR, CrossModalNet, and COFNet).

As shown in the left section of the Table I, SLGNet achieves the highest scores across all metrics, recording an mAP of 66.1, mAP_{50} of 98.3, and mAP_{75} of 75.4. Specifically, compared to the strongest unimodal IR baseline (YOLOv8), our method provides a significant gain of 4.0 points in mAP,

TABLE I

QUANTITATIVE COMPARISON WITH STATE-OF-THE-ART METHODS ON THE LLVIP AND FLIR DATASETS. THE BEST RESULTS ARE HIGHLIGHTED IN GREEN, AND THE SECOND-BEST RESULTS ARE MARKED IN PURPLE. "TRAINABLE PARAMS" REFERS TO THE NUMBER OF PARAMETERS UPDATED DURING TRAINING.

Methods	Modality	LLVIP			FLIR			Trainable Params
		mAP	mAP$_{50}$	mAP$_{75}$	mAP	mAP$_{50}$	mAP$_{75}$	
FasterRCNN [56]	IR	54.5	94.6	57.6	37.6	75.8	31.6	68.5M
RetinaNet [57]	IR	55.1	94.8	57.6	31.5	66.1	25.3	43.0M
YOLOV8 [58]	IR	62.1	95.2	67.0	38.3	72.9	31.8	76.7M
DDQ-DETR [59]	IR	58.6	93.9	64.6	37.1	73.9	32.2	244.6M
FasterRCNN [56]	RGB	45.1	87.0	41.2	27.7	62.2	21.2	68.5M
RetinaNet [57]	RGB	42.8	88.0	34.4	21.9	51.2	15.2	43.0M
YOLOV8 [58]	RGB	54.0	91.9	52.5	28.2	66.3	24.2	76.7M
DDQ-DETR [59]	RGB	46.7	86.1	45.8	30.9	64.9	24.5	244.6M
ICAFusion [21]	RGB+IR	-	-	-	41.4	79.2	36.9	120.0M
RSDet [24]	RGB+IR	61.3	95.8	70.4	43.8	83.9	40.1	-
UniRGB-IR [16]	RGB+IR	63.2	96.1	72.2	44.1	81.4	40.2	8.9M
CrossModalNet [22]	RGB+IR	64.7	97.7	73.5	43.3	81.7	39.1	92.8M
COFNet [23]	RGB+IR	65.9	97.7	75.9	44.6	83.6	41.7	90.2M
SLGNet (Ours)	RGB+IR	66.1	98.3	75.4	45.1	85.8	42.3	12.1M

demonstrating the necessity of multimodal fusion. Furthermore, against the runner-up multimodal method COFNet, SLGNet improves mAP$_{50}$ by 0.6 points. It is worth noting that SLGNet achieves this performance using only 12.1M trainable parameters, whereas COFNet requires 90.2M parameters, indicating a superior balance between accuracy and efficiency.

This performance advantage can be attributed to the synergistic design of our architecture. In dark environments where visual textures are lost, the Structure-Aware Adapter explicitly extracts edge priors from the thermal modality to compensate for the invisible visual cues. Simultaneously, the Language-Guided Modulation identifies the low-light context and recalibrates the feature channels to suppress noise from the RGB branch. This allows the model to maintain precise localization capabilities, as evidenced by the high mAP$_{50}$ score.

2) Comparisons on FLIR Dataset: The right section of Table I reports the detection performance on the FLIR dataset. Unlike LLVIP, FLIR features complex outdoor scenes with cluttered backgrounds, significant scale variations, and partial occlusions, which demand high generalization capabilities from the detector.

SLGNet demonstrates robust adaptability in this diverse environment, achieving the best performance across all metrics with an mAP of 45.1 and mAP$_{50}$ of 85.8. Notably, our method outperforms the competitive baseline COFNet by a margin of 2.2 points in mAP$_{50}$ and 0.5 points in mAP. When compared to CrossModalNet, the lead extends to 4.1 points in mAP$_{50}$. These improvements highlight the effectiveness of our multi-scale structural prior injection. While standard transformer-based methods often struggle to preserve fine-grained details due to fixed patch resolutions, our Structure Encoder captures spatial cues at multiple scales, enabling accurate detection of objects ranging from distant bicycles to nearby cars.

In terms of parameter efficiency, SLGNet achieves top-tier results with a remarkably compact trainable footprint. Our model requires only 12.1M trainable parameters, which represents a reduction of approximately 95% and 90% com-

TABLE II

QUANTITATIVE COMPARISON OF MULTIMODAL DETECTION PERFORMANCE ON THE KAIST DATASET. THE METRIC IS LOG-AVERAGE MISS RATE (MR^{-2}), WHERE LOWER IS BETTER. BEST AND SECOND-BEST RESULTS ARE HIGHLIGHTED IN GREEN AND PURPLE, RESPECTIVELY.

Methods	Backbone	MR^{-2}(%) ↓		
		All	Day	Night
ACF [60]	VGG-16	67.74	64.31	75.06
HalfwayFusion [7]	VGG-16	49.18	47.58	52.35
IATDNN+IASS [61]	VGG-16	48.96	49.02	49.37
CLAN [8]	VGG-16	35.53	36.02	32.38
AR-CNN [29]	VGG-16	34.95	34.36	36.12
MBNet [30]	ResNet-50	31.87	32.37	30.95
CMPD [27]	ResNet-50	28.98	28.30	30.56
CAGTDet [62]	ResNet-50	28.96	27.73	28.79
C2Former [33]	ResNet-50	28.39	28.48	26.67
UniRGB [16]	ViT-B	25.21	23.95	25.93
M-SpecGene [63]	ViT-B	23.74	25.66	19.42
SLGNet (Ours)	ViT-B	19.88	21.01	20.56

pared to heavy fusion models like DDQ-DETR (244.6M) and ICAFusion (120.0M), respectively. By freezing the ViT backbone and employing lightweight adapters, SLGNet proves that parameter-efficient tuning can yield state-of-the-art performance while avoiding the massive computational overhead associated with full-parameter fine-tuning.

3) Comparison on the KAIST Dataset: Table II details the pedestrian detection performance on the KAIST dataset. This benchmark presents unique challenges, including frequent spatial misalignment between modalities and drastic illumination changes between day and night.

SLGNet achieves a new state-of-the-art result with an overall MR^{-2} of 19.88. Compared to the strong ResNet-based baseline C2Former, which records a miss rate of 28.39, our method reduces the miss rate by 8.51 points, corresponding to a relative reduction of approximately 30.0%. Furthermore, against the recent ViT-based competitor M-SpecGene, SLGNet

TABLE III

QUANTITATIVE RESULTS ON THE DRONEVEHICLE DATASET USING THE mAP METRIC. THE BEST AND SECOND-BEST RESULTS ARE HIGHLIGHTED IN GREEN AND PURPLE, RESPECTIVELY.

Methods	mAP	Car	Truck	Freight-Car	Bus	Van
Halfway Fusion [7]	70.0	90.1	62.3	58.5	89.1	49.8
MBNet [64]	71.9	90.1	64.4	62.4	88.8	53.6
TSFADet [65]	73.1	89.9	67.9	63.7	89.8	54.0
C²Former [33]	74.2	90.2	78.3	64.4	89.8	58.5
AFFCM [66]	76.6	90.2	73.4	64.9	89.9	64.9
MC-DETR [67]	76.9	94.8	76.7	60.4	91.1	61.4
M2FP [17]	78.7	95.7	76.2	64.7	92.1	64.7
DMM [34]	79.4	90.4	79.8	68.2	89.9	68.6
UniFusOD [3]	79.5	96.4	81.3	63.5	90.8	65.6
WaveMamba [9]	79.8	95.0	80.4	68.5	90.6	64.5
SLGNet (Ours)	80.7	96.1	80.9	69.4	91.8	65.3

yields an improvement of 3.86 points in the overall metric, demonstrating the superiority of the proposed adapter paradigm over standard fusion transformers.

A detailed breakdown of day and night scenarios further reveals the robustness of our approach. In the daytime setting, SLGNet significantly outperforms all competitors with an MR^{-2} of 21.01. This score surpasses the second-best method UniRGB by 2.94 points and M-SpecGene by 4.65 points. Such a substantial lead in daytime scenarios suggests that the Structure-Aware Adapter effectively extracts critical edge cues even when thermal contrast is low, which is a common issue in daytime infrared images.

In the nighttime setting, SLGNet achieves a highly competitive MR^{-2} of 20.56, ranking second only to M-SpecGene which achieves 19.42. However, it is important to note the performance balance. While M-SpecGene shows a specific bias towards nighttime performance, its daytime error rate increases significantly to 25.66. In contrast, SLGNet maintains consistent and balanced accuracy across both illumination domains. These results indicate that SLGNet successfully mitigates the impact of modality misalignment and lighting variations. The consistent performance improvements validate that combining structure-aware structural priors with language-guided semantic modulation enables the model to generalize effectively across diverse temporal and environmental conditions.

4) Comparison on DroneVehicle Dataset: Table III reports the detection performance of various multi-modal methods on the DroneVehicle dataset. This benchmark focuses on aerial imagery captured by drones, introducing significant challenges such as abrupt viewing angle changes, arbitrary object orientations, and small object scales.

SLGNet demonstrates superior robustness in this aerial domain, achieving a state-of-the-art mAP of 80.7. This result surpasses the competitive baseline WaveMamba by 0.9 points and UniFusOD by 1.2 points. The consistent performance gains confirm that our framework, designed for robust cross-modal object detection, generalizes effectively from standard ground-level perspectives to challenging top-down aerial views without requiring specific architectural modifications.

A category-level analysis reveals the specific strengths of our proposed method. SLGNet achieves the highest score of 69.4 on the *Freight-Car* category, outperforming the second-

TABLE IV

COMPONENT-WISE ABLATION STUDY ON THE FLIR AND DRONEVEHICLE DATASETS. WE INCREMENTALLY ADD THE STRUCTURE-AWARE ADAPTER (SA-ADAPTER) AND LANGUAGE-GUIDED MODULATION (LGM) TO THE BASELINE. "Δ" DENOTES THE PERFORMANCE GAIN OF OUR FULL MODEL RELATIVE TO THE BASELINE.

Method	FLIR		DroneVehicle	
	mAP	mAP$_{50}$	mAP	mAP$_{50}$
Baseline	42.3	79.7	53.8	76.7
+ SA-Adapter	44.3	82.4	55.1	78.6
+ LGM	45.1	85.8	57.2	80.7
Δ	+2.8	+6.1	+3.4	+4.0

best method WaveMamba by 0.9 points. Freight cars typically exhibit distinct, elongated rectangular structures and prominent thermal signatures compared to the background. The superior performance in this category validates that our Structure-Aware Adapter successfully captures these long-range structural priors, effectively distinguishing large vehicles from complex backgrounds.

However, we observe a slight performance dip in the *Van* category, where SLGNet achieves 65.3, trailing behind DMM which scores 68.6. This can be attributed to the high visual ambiguity of vans in aerial views, where they often lack the distinct structural edges of trucks or freight cars and can be easily confused with large passenger cars. While our model heavily relies on explicit structural cues, methods like DMM may leverage more flexible, albeit less interpretable, feature interactions to handle such ambiguous classes. Nevertheless, SLGNet maintains a highly competitive overall performance, striking a balance between precise structure extraction for large objects and semantic understanding for general categories.

D. Ablation Study

1) Impact of Key Components: To quantify the individual contributions of the Structure-Aware Adapter (SA-Adapter) and Language-Guided Modulation (LGM), we incrementally incorporate these components into a baseline model. The baseline is constructed by concatenating RGB and IR inputs at the pixel level and feeding them into a frozen ViT backbone, where only the patch embedding layer and detection head are

TABLE V
COMPARISON OF PARAMETER EFFICIENCY AND DETECTION
PERFORMANCE BETWEEN FULL FINE-TUNING AND OUR
ADAPTER-TUNING PARADIGM ON THE FLIR AND DRONEVEHICLE
DATASETS. "PARAMS" DENOTES THE NUMBER OF TRAINABLE
PARAMETERS, AND "Δ" INDICATES THE RELATIVE IMPROVEMENT
ACHIEVED BY OUR PARADIGM.

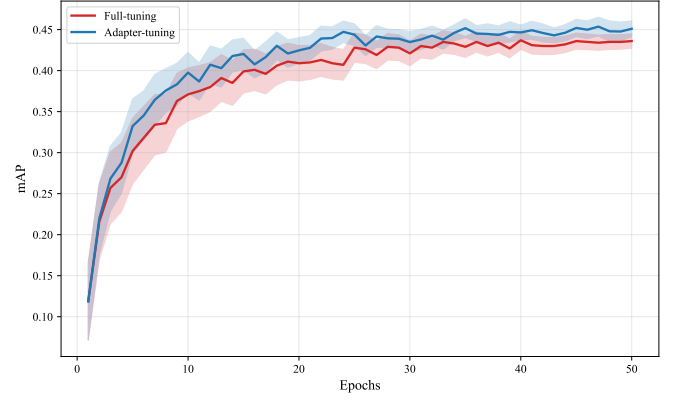| Tuning	Params	FLIR		DroneVehicle	
		mAP	mAP_{50}	mAP	mAP_{50}
Full-tuning	96.0M	43.6	82.2	53.5	75.3
Adapter-tuning	12.1M	45.1	85.8	57.2	80.7
Δ	-87%	+1.5	+3.6	+3.7	+5.4

Fig. 4. Validation mAP curves over training epochs on the FLIR dataset. The solid lines represent the mean mAP, while the shaded regions indicate the standard deviation range. The blue curve (Adapter-tuning) demonstrates faster convergence and higher stability (narrower error band) compared to the red curve (Full-tuning), confirming the robustness of our optimization strategy.

trainable. This setup serves as a controlled reference to strictly isolate the impact of our proposed modules.

Integrating the SA-Adapter yields significant performance gains, verifying the necessity of structural prior injection. As shown in Table IV, the inclusion of this module improves mAP by 2.0 points on FLIR and 1.3 points on DroneVehicle. This improvement addresses a critical limitation of the frozen ViT backbone, which, due to its $1/16$ spatial reduction, often loses high-frequency details essential for localization. By leveraging multi-scale structural priors such as edge cues, the SA-Adapter refines object boundaries and improves localization precision.

The subsequent addition of the LGM module further elevates performance by introducing scene-level semantic understanding. On the FLIR dataset, adding LGM results in a substantial leap in mAP_{50} (from 82.4 to 85.8), suggesting that language-driven contexts (e.g., distinguishing crowded backgrounds) play a pivotal role in reducing false positives. Ultimately, the full SLGNet achieves a total gain of 2.8 mAP on FLIR and 3.4 mAP on DroneVehicle compared to the baseline. These results demonstrate a synergistic effect: the SA-Adapter ensures structural integrity, while LGM provides semantic adaptability, jointly driving the model to state-of-the-art performance.

2) Impact of Structure-Aware Adapter: We conduct a two-fold analysis to evaluate the Structure-Aware Adapter (SA-Adapter) from the perspectives of training efficiency and feature interpretability.

Training Efficiency and Stability. We first compare our adapter-tuning paradigm with the traditional Full Fine-Tuning (FFT) strategy. As summarized in Table V, the proposed adapter-based approach demonstrates superior parameter efficiency, requiring only 12.1M trainable parameters—an approximate 87% reduction compared to the 96.0M parameters required for the full model. Despite this compact footprint, our method consistently outperforms FFT across both datasets. For instance, on the DroneVehicle dataset, Adapter-tuning achieves a remarkable gain of 5.4 points in mAP_{50} compared to full fine-tuning.

To further analyze the optimization dynamics, we visualize the validation mAP curves and their standard deviation intervals on the FLIR dataset in Fig. 4. As observed, the FFT curve (red) exhibits slower convergence and larger performance fluctuations, indicated by the wider shaded error bands. In contrast, our Adapter-tuning strategy (blue) converges rapidly

within the first 10 epochs and maintains a stable trajectory with a narrower standard deviation. This demonstrates that freezing the backbone and optimizing only the lightweight SA-Adapter effectively regularizes the optimization landscape, preventing the overfitting often associated with fine-tuning large vision transformers on smaller multimodal datasets.

Visualization of Structural Injection. To intuitively understand how the SA-Adapter refines features, we visualize the intermediate representations in Fig. 5. The reference structure map ∇_{ref} (Fig. 5(c)), derived from the maximum response of RGB and IR gradients, clearly highlights object contours that serve as the geometric guidance for our adapter.

Figs. 5(d)-(f) display the similarity maps of the final ViT features relative to three distinct query points (marked in red). It is evident that the attention focus is not limited to the local vicinity of the query pixels but spreads coherently along the structural boundaries of the objects. For the pedestrian (d) and the car (e), the high-response regions align perfectly with their semantic shapes, suppressing background noise.

A particularly compelling result is observed in Fig. 5(f), where the query point is placed on a *street light*—a background object that typically lacks bounding box annotations in detection datasets. Despite the absence of explicit supervision, the SA-Adapter successfully activates the entire pole structure. This confirms that the module has learned generic structural priors rather than merely overfitting to labeled categories, enabling the model to perceive scene geometry with high fidelity.

3) Impact of Text Encoder: To investigate how the semantic quality of text embeddings influences the modulation process, we compare the performance of SLGNet equipped with various pre-trained text encoders. As shown in Table VI, we evaluate three representative pure NLP models (BERT, T5, RoBERTa) and two vision-language models (BLIP, CLIP) on the FLIR and DroneVehicle datasets.

A clear performance gap is observed between pure language models and vision-language models. The NLP-based encoders, such as BERT and RoBERTa, yield suboptimal results, with mAP scores hovering around 43.2-43.6 on FLIR and 51.4-52.2
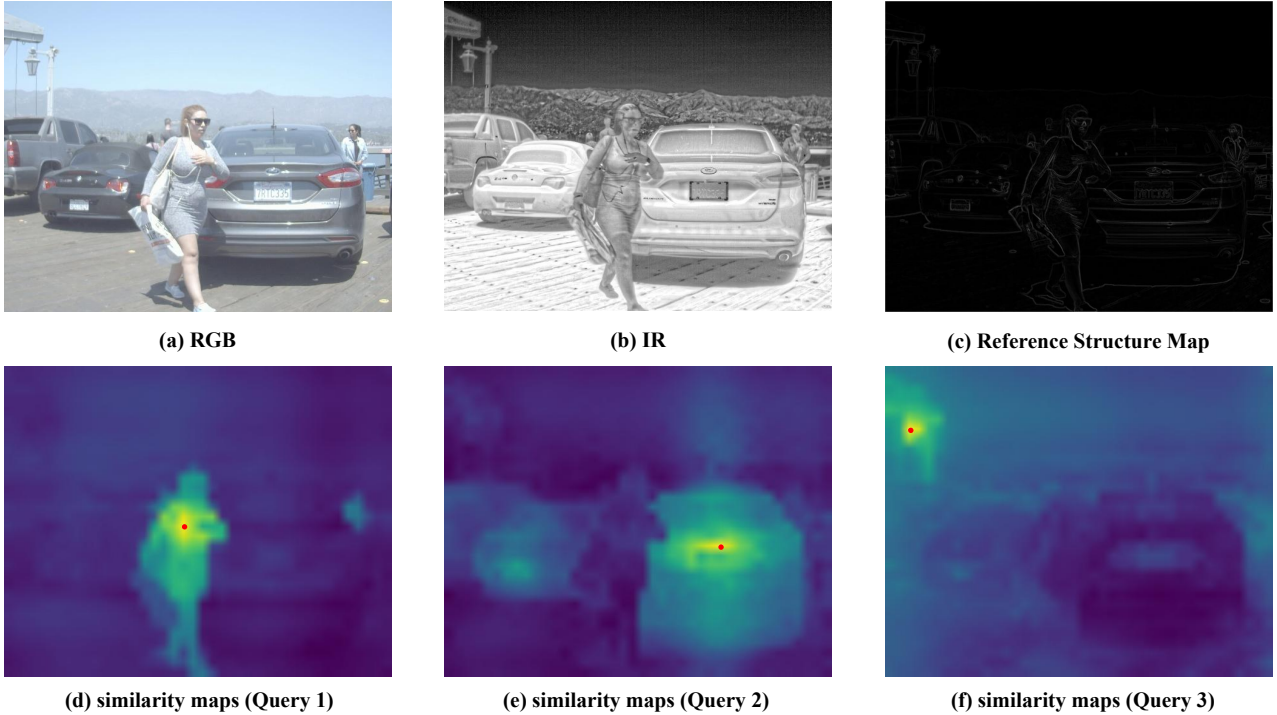
(a) RGB　　　　**(b) IR**　　　　**(c) Reference Structure Map**

(d) similarity maps (Query 1)　　**(e) similarity maps (Query 2)**　　**(f) similarity maps (Query 3)**

Fig. 5. Visualization of the structural feature learning process. (a)-(b) Input RGB and IR images. (c) The fused reference structure map (∇_{ref}). (d)-(f) **Cosine similarity maps** computed between the feature of the query patch (marked as •) and all other patches in the adapted ViT output. The high similarity spreading coherently along structural boundaries (e.g., the pedestrian in (d) and the unannotated street light in (f)) demonstrates that the SA-Adapter effectively injects structural priors into the semantic feature space.

TABLE VI
PERFORMANCE COMPARISON OF DIFFERENT TEXT ENCODERS UTILIZED IN THE LANGUAGE-GUIDED MODULATION MODULE. THE SUPERIOR PERFORMANCE OF VISION-LANGUAGE MODELS (BLIP, CLIP) HIGHLIGHTS THE IMPORTANCE OF CROSS-MODAL ALIGNMENT.

Text Encoder	FLIR		DroneVehicle	
	mAP	mAP$_{50}$	mAP	mAP$_{50}$
BERT [68]	43.2	81.9	51.4	72.5
T5 [69]	43.8	83.0	51.8	73.6
RoBERTa [70]	43.6	82.2	52.2	73.6
BLIP [42]	44.9	84.8	56.1	79.8
CLIP [40]	**45.1**	**85.8**	**57.2**	**80.7**

TABLE VII
ABLATION STUDY ON THE GRANULARITY OF TEXT PROMPTS USED IN LGM. "CONCATENATED CATS" USES A FIXED SENTENCE LISTING ALL OBJECT CATEGORIES; "UNSTRUCTURED" DENOTES FREE-FORM CAPTIONS; "STRUCTURED" IS OUR PROPOSED HIERARCHICAL DESCRIPTION.

Prompt Strategy	FLIR		DroneVehicle	
	mAP	mAP$_{50}$	mAP	mAP$_{50}$
Concatenated Cats.	43.9	82.0	55.4	78.8
Unstructured Caption	44.7	84.5	56.3	79.9
Structured Caption (Ours)	**45.1**	**85.8**	**57.2**	**80.7**

on DroneVehicle. While these models possess strong linguistic understanding, their feature spaces are constructed solely from text corpora. Consequently, there exists a significant semantic gap between their textual embeddings and the visual features extracted by the ViT backbone, making it difficult for the LGM module to effectively modulate visual channels based on text prompts.

In contrast, encoders pre-trained on large-scale image-text pairs (BLIP and CLIP) demonstrate superior performance. CLIP achieves the highest accuracy across all metrics, recording an mAP of 45.1 on FLIR and 57.2 on DroneVehicle. This advantage stems from the contrastive pre-training of CLIP, which explicitly aligns the visual and textual embedding spaces. This alignment ensures that the semantic vectors for prompts like "car" or "thermal signature" are mathematically

close to their corresponding visual features, thereby maximizing the effectiveness of the semantic modulation and guiding the detector to focus on contextually relevant regions.

4) Impact of Prompt Granularity: To justify the necessity of our structured prompt design, we evaluate the impact of different prompt granularity levels on detection performance. We compare our approach against two baselines: (1) **Concatenated Categories**, which uses a static template listing all target classes; and (2) **Unstructured Caption**, where the VLM generates a free-form description.

As presented in Table VII, utilizing simple *Concatenated Categories* results in suboptimal performance, yielding an mAP of 43.9 on FLIR. Crucially, this score is slightly lower than the model without the LGM module (44.3 mAP, see Table IV), indicating that static prompts consisting solely of class names introduce semantic noise. Without environmental
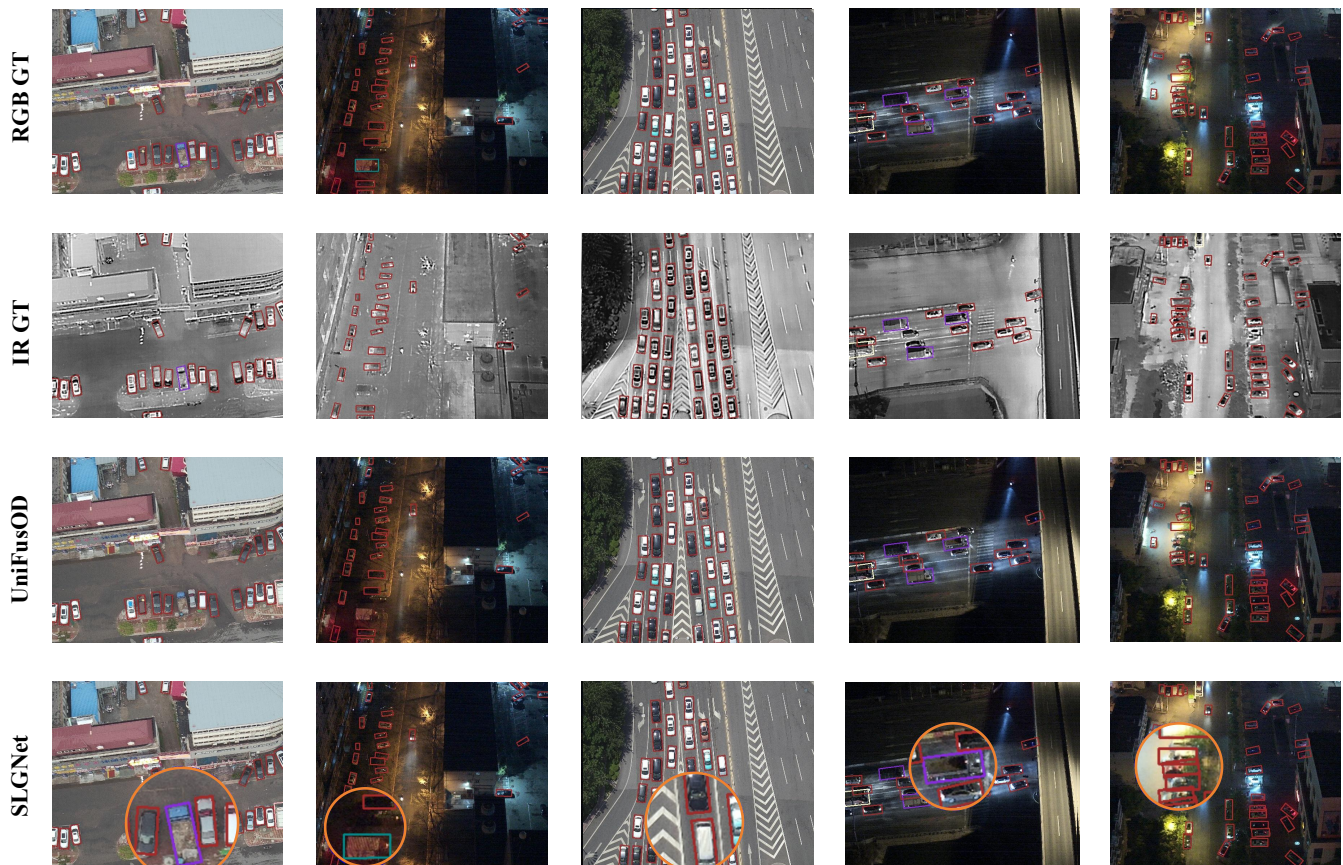
Fig. 6. Visualization of detection results on the **DroneVehicle** dataset. The first and second rows display the Ground Truth (GT) annotations for RGB and Infrared (IR) images, respectively. The third row presents the results from the state-of-the-art method UniFusOD [3], while the fourth row shows the results of our proposed SLGNet. The blue dashed boxes highlight magnified regions, demonstrating that SLGNet significantly outperforms the baseline in detecting small, densely packed vehicles typical in aerial surveillance scenarios.

context, these prompts fail to provide actionable modulation signals, instead interfering with the pre-trained visual features.

Moving to *Unstructured Captions* brings a performance gain, raising the mAP to 44.7 on FLIR. This suggests that generic scene descriptions can capture useful context (e.g., distinguishing street scenes). However, the proposed Structured Caption achieves the superior results, outperforming the unstructured variant by 0.4 mAP on FLIR and 0.9 mAP on DroneVehicle. The improvement is most notable in mAP_{50} (reaching 85.8), demonstrating that explicitly encoding domain-specific priors—such as s_{env} (e.g., "low-light") and s_{therm} (e.g., "high thermal contrast")—is essential. By structuring the prompt to enforce these attributes, we ensure the LGM module receives precise, consistent signals to optimize feature fusion in complex multimodal scenarios.

E. Qualitative Analysis

To intuitively evaluate the robustness of SLGNet in aerial surveillance scenarios, we provide visualization comparisons on the DroneVehicle dataset in Fig. 6. This dataset presents unique challenges, including small object scales, high density, and complex background textures from a top-down perspective.

As shown in the third row, the competing method UniFusOD [3] exhibits limitations in these challenging conditions. Specifically, in the magnified regions (marked by blue dashed boxes), it fails to distinguish adjacent vehicles or misses small targets entirely due to the loss of fine-grained structural details during feature fusion.

In contrast, as depicted in the fourth row, our SLGNet accurately localizes these difficult targets, maintaining high consistency with the Ground Truth. This superior performance is largely attributed to the Structure-Aware Adapter, which effectively recovers high-frequency edge cues (e.g., vehicle contours) that are critical for separating densely packed objects in aerial views. Furthermore, the Language-Guided Modulation aids in suppressing background noise, ensuring the model focuses on valid target regions. These visual results corroborate the quantitative improvements reported in Table III, confirming the effectiveness of our framework in maintaining geometric integrity and semantic accuracy.

V. CONCLUSION

In this paper, we presented SLGNet, a parameter-efficient framework that synergizes structural recovery with semantic reasoning to bridge the gap between foundation mod-

els and robust multimodal object detection. By combining a Structure-Aware Adapter for geometric localization and Language-Guided Modulation (LGM) for environmental adaptation, our approach addresses the structural degradation of frozen backbones while equipping the model with scene-level awareness. Extensive experiments demonstrate that SLGNet establishes new state-of-the-art results with superior parameter efficiency. Future work will explore cloud-edge collaborative architectures to mitigate VLM inference overhead. We aim to implement an asynchronous execution strategy where cloud-resident VLMs periodically update semantic priors to guide real-time edge detectors. We hope this paradigm provides new insights for integrating large foundation models into real-time sensing, potentially fostering a better balance between high-level reasoning and industrial-scale efficiency.

REFERENCES

[1] Y. Choi, N. Kim, S. Hwang, K. Park, J. S. Yoon, K. An, and I. S. Kweon, "Kaist multi-spectral day/night data set for autonomous and assisted driving," *IEEE Transactions on Intelligent Transportation Systems*, vol. 19, no. 3, pp. 934–948, 2018.

[2] Y. Sun, B. Cao, P. Zhu, and Q. Hu, "Drone-based rgb-infrared cross-modality vehicle detection via uncertainty-aware learning," *IEEE Transactions on Circuits and Systems for Video Technology*, vol. 32, no. 10, pp. 6700–6713, 2022.

[3] X. Xiang, G. Zhou, B. Niu, Z. Pan, L. Huang, W. Li, Z. Wen, J. Qi, and W. Gao, "Infrared-visible image fusion meets object detection: Towards unified optimization for multimodal perception," *Remote Sensing*, vol. 17, no. 21, p. 3637, 2025.

[4] Q. Ha, K. Watanabe, T. Karasawa, Y. Ushiku, and T. Harada, "Mfnet: Towards real-time semantic segmentation for autonomous vehicles with multi-spectral scenes," in *2017 IEEE/RSJ International Conference on Intelligent Robots and Systems (IROS)*. IEEE, 2017, pp. 5108–5115.

[5] C. Li, D. Song, R. Tong, and M. Tang, "Illumination-aware faster r-cnn for robust multispectral pedestrian detection," *Pattern Recognition*, vol. 85, pp. 161–171, 2019.

[6] Z. Wen, P. Li, Y. Liu, J. Chen, X. Xiang, Y. Li, H. Wang, Y. Zhao, and G. Zhou, "Fanet: Frequency-aware attention-based tiny-object detection in remote sensing images," *Remote Sensing*, 2025.

[7] J. Liu, S. Zhang, S. Wang, and D. N. Metaxas, "Multispectral deep neural networks for pedestrian detection," *arXiv preprint arXiv:1611.02644*, 2016.

[8] L. Zhang, Z. Liu, S. Zhang, X. Yang, H. Qiao, K. Huang, and A. Hussain, "Cross-modality interactive attention network for multispectral pedestrian detection," *Information Fusion*, vol. 50, pp. 20–29, 2019.

[9] H. Zhu, W. Dong, L. Yang, H. Li, Y. Yang, Y. Ren, Q. Zhu, Z. Feng, C. Li, S. Lin *et al.*, "Wavemamba: Wavelet-driven mamba fusion for rgb-infrared object detection," in *Proceedings of the IEEE/CVF International Conference on Computer Vision*, 2025, pp. 11 219–11 229.

[10] A. Dosovitskiy, "An image is worth 16x16 words: Transformers for image recognition at scale," *arXiv preprint arXiv:2010.11929*, 2020.

[11] M. Caron, H. Touvron, I. Misra, H. Jégou, J. Mairal, P. Bojanowski, and A. Joulin, "Emerging properties in self-supervised vision transformers," in *Proceedings of the IEEE/CVF international conference on computer vision*, 2021, pp. 9650–9660.

[12] M. Oquab, T. Darcet, T. Moutakanni, H. Vo, M. Szafraniec, V. Khalidov, P. Fernandez, D. Haziza, F. Massa, A. El-Nouby *et al.*, "Dinov2: Learning robust visual features without supervision," *arXiv preprint arXiv:2304.07193*, 2023.

[13] O. Siméoni, H. V. Vo, M. Seitzer, F. Baldassarre, M. Oquab, C. Jose, V. Khalidov, M. Szafraniec, S. Yi, M. Ramamonjisoa *et al.*, "Dinov3," *arXiv preprint arXiv:2508.10104*, 2025.

[14] A. Kirillov, E. Mintun, N. Ravi, H. Mao, C. Rolland, L. Gustafson, T. Xiao, S. Whitehead, A. C. Berg, W.-Y. Lo *et al.*, "Segment anything," in *Proceedings of the IEEE/CVF international conference on computer vision*, 2023, pp. 4015–4026.

[15] H. R. Medeiros, D. Latortue, E. Granger, and M. Pedersoli, "Mixed patch visible-infrared modality agnostic object detection," in *2025 IEEE/CVF Winter Conference on Applications of Computer Vision (WACV)*. IEEE, 2025, pp. 9023–9032.

[16] M. Yuan, B. Cui, T. Zhao, J. Wang, S. Fu, X. Yang, and X. Wei, "Unirgb-ir: A unified framework for visible-infrared semantic tasks via adapter tuning," in *Proceedings of the 33rd ACM International Conference on Multimedia*, 2025, pp. 2409–2418.

[17] J. Ouyang, P. Jin, and Q. Wang, "Multimodal feature-guided pre-training for rgb-t perception," *IEEE Journal of Selected Topics in Applied Earth Observations and Remote Sensing*, 2024.

[18] V. V. Ramasesh, A. Lewkowycz, and E. Dyer, "Effect of scale on catastrophic forgetting in neural networks," in *International conference on learning representations*, 2021.

[19] Z. Chen, Y. Duan, W. Wang, J. He, T. Lu, J. Dai, and Y. Qiao, "Vision transformer adapter for dense predictions," *arXiv preprint arXiv:2205.08534*, 2022.

[20] Z. Han, C. Gao, J. Liu, J. Zhang, and S. Q. Zhang, "Parameter-efficient fine-tuning for large models: A comprehensive survey," *arXiv preprint arXiv:2403.14608*, 2024.

[21] J. Shen, Y. Chen, Y. Liu, X. Zuo, H. Fan, and W. Yang, "Icafusion: Iterative cross-attention guided feature fusion for multispectral object detection," *Pattern Recognition*, vol. 145, p. 109913, 2024.

[22] H. Li, L. Xiao, L. Cao, D. Wu, Y. Liu, Y. Li, Y. Zhang, and H. Bao, "Crossmodalnet: A dual-modal object detection network based on cross-modal fusion and channel interaction," *Expert Systems with Applications*, p. 129677, 2025.

[23] M. Zhou, Y. Li, G. Yang, X. Wei, H. Pu, J. Luo, and W. Jia, "Cofnet: Contrastive object-aware fusion using box-level masks for multispectral object detection," *IEEE Transactions on Multimedia*, 2025.

[24] T. Zhao, M. Yuan, F. Jiang, N. Wang, and X. Wei, "Removal and selection: Improving rgb-infrared object detection via coarse-to-fine fusion," *arXiv preprint arXiv:2401.10731*, 2024.

[25] Z. Huang, J. Liu, L. Li, K. Zheng, and Z.-J. Zha, "Modality-adaptive mixup and invariant decomposition for rgb-infrared person re-identification," in *Proceedings of the AAAI conference on artificial intelligence*, vol. 36, no. 1, 2022, pp. 1034–1042.

[26] M. Ye, W. Ruan, B. Du, and M. Z. Shou, "Channel augmented joint learning for visible-infrared recognition," in *Proceedings of the IEEE/CVF international conference on computer vision*, 2021, pp. 13 567–13 576.

[27] Q. Li, C. Zhang, Q. Hu, H. Fu, and P. Zhu, "Confidence-aware fusion using dempster-shafer theory for multispectral pedestrian detection," *IEEE Transactions on Multimedia*, vol. 25, pp. 3420–3431, 2022.

[28] J. Yang, X. Yang, Y. Liao, J. Huang, H. He, E. Zhang, Y. Zhou, and Y. Song, "Multispectral sample augmentation and illumination guidance for rgb-t object detection by mm detection framework," in *4th International Conference on Laser, Optics, and Optoelectronic Technology (LOPET 2024)*, vol. 13231. SPIE, 2024, pp. 538–544.

[29] L. Zhang, X. Zhu, X. Chen, X. Yang, Z. Lei, and Z. Liu, "Weakly aligned cross-modal learning for multispectral pedestrian detection," in *Proceedings of the IEEE/CVF international conference on computer vision*, 2019, pp. 5127–5137.

[30] K. Zhou, L. Chen, and X. Cao, "Improving multispectral pedestrian detection by addressing modality imbalance problems," in *European conference on computer vision*. Springer, 2020, pp. 787–803.

[31] S. Peng, X. Zhu, H. Deng, L.-J. Deng, and Z. Lei, "Fusionmamba: Efficient remote sensing image fusion with state space model," *IEEE Transactions on Geoscience and Remote Sensing*, 2024.

[32] J. Guo, C. Gao, F. Liu, D. Meng, and X. Gao, "Damsdet: Dynamic adaptive multispectral detection transformer with competitive query selection and adaptive feature fusion," in *European Conference on Computer Vision*. Springer, 2024, pp. 464–481.

[33] M. Yuan and X. Wei, "C^{2}former: Calibrated and complementary transformer for rgb-infrared object detection," *IEEE Transactions on Geoscience and Remote Sensing*, vol. 62, pp. 1–12, 2024.

[34] M. Zhou, T. Li, C. Qiao, D. Xie, G. Wang, N. Ruan, L. Mei, Y. Yang, and H. T. Shen, "Dmm: Disparity-guided multispectral mamba for oriented object detection in remote sensing," *IEEE Transactions on Geoscience and Remote Sensing*, 2025.

[35] N. Houlsby, A. Giurgiu, S. Jastrzebski, B. Morrone, Q. De Laroussilhe, A. Gesmundo, M. Attariyan, and S. Gelly, "Parameter-efficient transfer learning for nlp," in *International conference on machine learning*. PMLR, 2019, pp. 2790–2799.

[36] E. J. Hu, Y. Shen, P. Wallis, Z. Allen-Zhu, Y. Li, S. Wang, L. Wang, W. Chen *et al.*, "Lora: Low-rank adaptation of large language models." *ICLR*, vol. 1, no. 2, p. 3, 2022.

[37] M. Jia, L. Tang, B.-C. Chen, C. Cardie, S. Belongie, B. Hariharan, and S.-N. Lim, "Visual prompt tuning," in *European conference on computer vision*. Springer, 2022, pp. 709–727.

[38] S. Lee, S. Park, D. B. Lee, D. Wagner, H. Seong, T. Bocklet, J. Lee, and S. J. Hwang, "Fedsvd: Adaptive orthogonalization for private federated learning with lora," *arXiv preprint arXiv:2505.12805*, 2025.

[39] S. Chen, C. Ge, Z. Tong, J. Wang, Y. Song, J. Wang, and P. Luo, "Adaptformer: Adapting vision transformers for scalable visual recognition," *Advances in Neural Information Processing Systems*, vol. 35, pp. 16 664–16 678, 2022.

[40] A. Radford, J. W. Kim, C. Hallacy, A. Ramesh, G. Goh, S. Agarwal, G. Sastry, A. Askell, P. Mishkin, J. Clark *et al.*, "Learning transferable visual models from natural language supervision," in *International conference on machine learning*. PmLR, 2021, pp. 8748–8763.

[41] C. Jia, Y. Yang, Y. Xia, Y.-T. Chen, Z. Parekh, H. Pham, Q. Le, Y.-H. Sung, Z. Li, and T. Duerig, "Scaling up visual and vision-language representation learning with noisy text supervision," in *International conference on machine learning*. PMLR, 2021, pp. 4904–4916.

[42] J. Li, D. Li, S. Savarese, and S. Hoi, "Blip-2: Bootstrapping language-image pre-training with frozen image encoders and large language models," in *International conference on machine learning*. PMLR, 2023, pp. 19 730–19 742.

[43] H. Liu, C. Li, Q. Wu, and Y. J. Lee, "Visual instruction tuning," *Advances in neural information processing systems*, vol. 36, pp. 34 892–34 916, 2023.

[44] D. Zhu, J. Chen, X. Shen, X. Li, and M. Elhoseiny, "Minigpt-4: Enhancing vision-language understanding with advanced large language models," *arXiv preprint arXiv:2304.10592*, 2023.

[45] S. Bai, K. Chen, X. Liu, J. Wang, W. Ge, S. Song, K. Dang, P. Wang, S. Wang, J. Tang *et al.*, "Qwen2. 5-vl technical report," *arXiv preprint arXiv:2502.13923*, 2025.

[46] L. H. Li, P. Zhang, H. Zhang, J. Yang, C. Li, Y. Zhong, L. Wang, L. Yuan, L. Zhang, J.-N. Hwang *et al.*, "Grounded language-image pre-training," in *Proceedings of the IEEE/CVF conference on computer vision and pattern recognition*, 2022, pp. 10 965–10 975.

[47] S. Liu, Z. Zeng, T. Ren, F. Li, H. Zhang, J. Yang, Q. Jiang, C. Li, J. Yang, H. Su *et al.*, "Grounding dino: Marrying dino with grounded pre-training for open-set object detection," in *European conference on computer vision*. Springer, 2024, pp. 38–55.

[48] Y. Zhong, J. Yang, P. Zhang, C. Li, N. Codella, L. H. Li, L. Zhou, X. Dai, L. Yuan, Y. Li *et al.*, "Regionclip: Region-based language-image pretraining," in *Proceedings of the IEEE/CVF conference on computer vision and pattern recognition*, 2022, pp. 16 793–16 803.

[49] F. Liu, D. Chen, Z. Guan, X. Zhou, J. Zhu, Q. Ye, L. Fu, and J. Zhou, "Remoteclip: A vision language foundation model for remote sensing," *IEEE Transactions on Geoscience and Remote Sensing*, vol. 62, pp. 1–16, 2024.

[50] K. Kuckreja, M. S. Danish, M. Naseer, A. Das, S. Khan, and F. S. Khan, "Geochat: Grounded large vision-language model for remote sensing," in *Proceedings of the IEEE/CVF Conference on Computer Vision and Pattern Recognition*, 2024, pp. 27 831–27 840.

[51] X. Guo, J. Lao, B. Dang, Y. Zhang, L. Yu, L. Ru, L. Zhong, Z. Huang, K. Wu, D. Hu *et al.*, "Skysense: A multi-modal remote sensing foundation model towards universal interpretation for earth observation imagery," in *Proceedings of the IEEE/CVF Conference on Computer Vision and Pattern Recognition*, 2024, pp. 27 672–27 683.

[52] Y. Hu, J. Yuan, C. Wen, X. Lu, Y. Liu, and X. Li, "Rsgpt: A remote sensing vision language model and benchmark," *ISPRS Journal of Photogrammetry and Remote Sensing*, vol. 224, pp. 272–286, 2025.

[53] X. Zhu, W. Su, L. Lu, B. Li, X. Wang, and J. Dai, "Deformable detr: Deformable transformers for end-to-end object detection," *arXiv preprint arXiv:2010.04159*, 2020.

[54] X. Jia, C. Zhu, M. Li, W. Tang, and W. Zhou, "Llvip: A visible-infrared paired dataset for low-light vision," in *Proceedings of the IEEE/CVF international conference on computer vision*, 2021, pp. 3496–3504.

[55] H. Zhang, E. Fromont, S. Lefevre, and B. Avignon, "Multispectral fusion for object detection with cyclic fuse-and-refine blocks," in *2020 IEEE International conference on image processing (ICIP)*. IEEE, 2020, pp. 276–280.

[56] S. Ren, K. He, R. Girshick, and J. Sun, "Faster r-cnn: Towards real-time object detection with region proposal networks," *Advances in neural information processing systems*, vol. 28, 2015.

[57] T.-Y. Lin, P. Goyal, R. Girshick, K. He, and P. Dollár, "Focal loss for dense object detection," in *Proceedings of the IEEE international conference on computer vision*, 2017, pp. 2980–2988.

[58] G. Jocher, A. Chaurasia, and J. Qiu, "Ultralytics yolo," Jan. 2023. [Online]. Available: https://github.com/ultralytics/ultralytics

[59] S. Zhang, X. Wang, J. Wang, J. Pang, C. Lyu, W. Zhang, P. Luo, and K. Chen, "Dense distinct query for end-to-end object detection," in *Proceedings of the IEEE/CVF conference on computer vision and pattern recognition*, 2023, pp. 7329–7338.

[60] S. Hwang, J. Park, N. Kim, Y. Choi, and I. So Kweon, "Multispectral pedestrian detection: Benchmark dataset and baseline," in *Proceedings of the IEEE conference on computer vision and pattern recognition*, 2015, pp. 1037–1045.

[61] D. Guan, Y. Cao, J. Yang, Y. Cao, and M. Y. Yang, "Fusion of multispectral data through illumination-aware deep neural networks for pedestrian detection," *Information Fusion*, vol. 50, pp. 148–157, 2019.

[62] M. Yuan, X. Shi, N. Wang, Y. Wang, and X. Wei, "Improving rgb-infrared object detection with cascade alignment-guided transformer," *Information Fusion*, vol. 105, p. 102246, 2024.

[63] K. Zhou, F. Yang, S. Wang, B. Wen, C. Zi, L. Chen, Q. Shen, and X. Cao, "M-specgene: Generalized foundation model for rgbt multispectral vision," in *Proceedings of the IEEE/CVF International Conference on Computer Vision*, 2025, pp. 7861–7872.

[64] L. Shan and W. Wang, "Mbnet: A multi-resolution branch network for semantic segmentation of ultra-high resolution images," in *ICASSP 2022-2022 IEEE International Conference on Acoustics, Speech and Signal Processing (ICASSP)*. IEEE, 2022, pp. 2589–2593.

[65] M. Yuan, Y. Wang, and X. Wei, "Translation, scale and rotation: Cross-modal alignment meets rgb-infrared vehicle detection," in *European Conference on Computer Vision*. Springer, 2022, pp. 509–525.

[66] Y. Wu, X. Guan, B. Zhao, L. Ni, and M. Huang, "Vehicle detection based on adaptive multimodal feature fusion and cross-modal vehicle index using rgb-t images," *IEEE Journal of Selected Topics in Applied Earth Observations and Remote Sensing*, vol. 16, pp. 8166–8177, 2023.

[67] J. Ouyang, Q. Wang, J. Liu, X. Qu, J. Song, and T. Shen, "Multi-modal and cross-scale feature fusion network for vehicle detection with transformers," in *2023 International Conference on Machine Vision, Image Processing and Imaging Technology (MVIPIT)*. IEEE, 2023, pp. 175–180.

[68] J. Devlin, M.-W. Chang, K. Lee, and K. Toutanova, "Bert: Pre-training of deep bidirectional transformers for language understanding," in *Proceedings of the 2019 conference of the North American chapter of the association for computational linguistics: human language technologies, volume 1 (long and short papers)*, 2019, pp. 4171–4186.

[69] J. Ni, G. H. Abrego, N. Constant, J. Ma, K. Hall, D. Cer, and Y. Yang, "Sentence-t5: Scalable sentence encoders from pre-trained text-to-text models," in *Findings of the association for computational linguistics: ACL 2022*, 2022, pp. 1864–1874.

[70] Y. Liu, M. Ott, N. Goyal, J. Du, M. Joshi, D. Chen, O. Levy, M. Lewis, L. Zettlemoyer, and V. Stoyanov, "Roberta: A robustly optimized bert pretraining approach," *arXiv preprint arXiv:1907.11692*, 2019.